Noncatalytic Coal Char Gasification

A simple particle model is used to interpret differential thermogravimetric data taken on the gasification of coal/char with CO_2, H_2 and H_2O. The model takes into account the major physical factors which influence the gasification rate, *viz.*, the changing magnitudes of surface area, porosity, activation energy and effective diffusivity during gasification. Specific reaction rate constants based on surface area and activation energies are extracted from the data. Practical criteria for regimes of reaction rate and diffusion control and for particle isothermality are developed. For isothermal particles at low classical Thiele moduli, the data can be correlated with only one parameter, which has a simple physical interpretation.

SUNGGYU LEE, J. C. ANGUS, R. V. EDWARDS, and N. C. GARDNER

Chemical Engineering Department
Case Western Reserve University
Cleveland, OH 44106

SCOPE

Many theoretical and empirical models for the correlation of coal gasification kinetics have been proposed. These include essentially empirical correlations in which constants that have little relation to independently measurable quantities are chosen to give a best fit to the data. Other models do not take into account the evolution of physical properties as the carbonaceous matrix is consumed. Still others consider complex gas-phase kinetic processes, but are so complex that only difficult numerical solutions to the equations are possible.

In this work we take a different approach: 1) the effect of conversion of the carbonaceous material on the relevant physical properties; 2) use of constants in the model which have clear physical significance and which can be determined by independent measurements; and 3) maintaining sufficient mathematical simplicity so that asymptotic analytical solutions can be obtained in the regions of high and low (modified) Thiele moduli.

This approach is dictated by two considerations. First, the evolution of the physical structure (porosity, specific surface area, etc.) plays a dominant role in determining the reactivity of char. Second, there is a need for a model which can be used without recourse to numerical routines or to data which are normally unavailable and yet is sufficiently realistic to predict the principal features observed in char gasification kinetics. These latter features include: the existence of a so-called universal curve of char reactivity (Mahajan et al., 1978) and the observation of a maximum in the reaction rate at intermediate conversions (Feldkirchner and Huebler, 1965).

To achieve the above goals several restrictive assumptions must be made. Perhaps the most severe is to include all of the heterogeneous chemical kinetics into a single first-order rate expression. The justification for this is simply that in most practical situations the possible spectrum of species, the elementary molecular processes, and the appropriate kinetic constants are unknown. Another major assumption is the use of simple algebraic relationship among activation energy, effective diffusion coefficient, density, specific surface area and porosity (conversion). The effect of convective flow in the pores was also neglected.

CONCLUSIONS AND SIGNIFICANCE

A single particle model was developed and used to interpret kinetic data taken on the gasification of coal char with H_2, CO_2 and H_2O. The model takes into account the major physical factors which influence the gasification rate, *viz.*, the changing magnitudes of surface area, porosity, activation energy and effective diffusivity during gasification, but is sufficiently tractable mathematically to permit asymptotic analytical solutions for high and low Thiele moduli. Equations for both isothermal and nonisothermal particles were formulated and solved to obtain the local conversion-time relationship. Practical criteria for identification of the regimes of reaction rate or diffusion control and for particle isothermality were developed. The model, which only has two parameters, closely describes the shape of the conversion vs. time curves as determined by CO_2 gasification studies. Moreover, it describes the maximum in the rate sometimes observed at intermediate conversions and, under certain restrictions, leads to a "universal curve" of conversion vs. an appropriate dimensionless time.

The model was used to calculate activation energies and intrinsic rate constants (based on surface area) for CO_2 gasification of char. The intrinsic rate constants for various chars were very nearly the same at the same temperature and were close to the reported values for the CO_2 gasification of graphite. These results suggest that, despite its simplicity, the model does describe the major factors that influence the reactivity of chars.

Significant features of the model are its mathematical simplicity and the fact that the parameters have clear physical significance. The asymptotic solutions that were obtained for the limiting cases of low and high Thiele moduli can be used in reactor modelling studies thereby avoiding complex numerical routines.

ISOTHERMAL PARTICLE MODEL

Mathematical Formulation

Let a spherical char particle of initial radius R_o be exposed to a gas mixture containing steam (or hydrogen, carbon dioxide) whose bulk concentration is $C_{A,s}$. If the concentration of steam varies only in the radial direction, then the material balance on the steam is:

$$\frac{\partial \epsilon C_A}{\partial t} = \frac{1}{r^2}\frac{\partial}{\partial r}\left(r^2 D_e \frac{\partial C_A}{\partial r}\right) + \frac{\partial C_c}{\partial t} \tag{1}$$

Boundary conditions are:

$$C_A = C_{A,s} \text{ at } r = R \text{ and } \frac{\partial C_A}{\partial r} = 0 \text{ at } r = 0. \tag{2}$$

Sunggyu Lee is presently with the Department of Chemical Engineering, The University of Akron, Akron, OH 44325. Correspondence concerning this paper should be addressed to him.

Carbon gasification reactions at low to moderate pressures often have an empirical reaction order of between zero and one and appear to follow rate expressions of the Langmuir-Hinshelwood type. However, the order of reaction at high pressures can be greater than one (Blackwood and Ingeme, 1960). In this analysis the reaction is assumed to be first order in the gaseous concentration. The material balance for carbon then becomes

$$\frac{\partial C_c}{\partial t} = -kS_g\rho_p C_A. \tag{3}$$

In most previous work it has been assumed that the physical properties are independent of radius or remain constant during the reaction. This assumption is not realistic because as the particle reacts, the effective diffusion coefficient, the surface reaction rate constant, the specific surface area and the density all change locally, in some cases drastically.

For the effective diffusivity, D_e, the simplest empirical relationship is:

$$D_e = D\epsilon^2 \tag{4}$$

Other, more sophisticated, models give different results. For example, Petersen (1965) derived the porosity dependence of effective diffusivity using Maxwell's model and obtained an $\epsilon^{3/2}$ dependence. Whatever the model, D_e must vary with both time and position as the porosity varies.

As the internal void volume increases, the specific surface area initially increases. A linear dependence can be assumed in the range of moderate conversions (Walker et al., 1959),

$$S_g = S\epsilon \tag{5}$$

In the absence of swelling or shrinking of residual solid structure, the bulk and true densities of the particle are related:

$$\rho_p = \rho_t(1 - \epsilon) \tag{6}$$

If the porosity changes solely from the heterogeneous reaction, then porosity is directly related to fractional conversion. With this assumption for an ash-free particle one has:

$$\epsilon = 1 - (1 - \epsilon_0)(1 - x) \tag{7}$$

It should be noted that the pore structure can also change from swelling, shrinking, caking, etc.

The intrinsic reaction rate constant is a function of temperature and activation energy, the latter of which can also depend upon the carbon conversion. Since the local carbon conversion is directly related to porosity, i.e., Eq. 7, the activation energy is a function of porosity. In the absence of any other information, the simplest relation is a linear form

$$E = E_0(1 + \gamma'\epsilon) \tag{8}$$

Further, since the intrinsic rate constant can be expressed as an Arrhenius type equation,

$$k = A\exp(-E/RT) = A\exp\{-E_0(1 + \gamma'\epsilon)/RT\} \cong k_0(1 - \gamma\epsilon) \tag{9}$$

where γ is a constant different from γ' and can be approximated by $\gamma = E_0\gamma'/RT$ if γ' is sufficiently small.

Substituting Eqs. 5, 6 and 9 into Eq. 3 and combining Eqs. 3, 4 and 1, one obtains the steam and carbon balances in the following dimensionless form:

$$h^2\frac{\partial \epsilon C_A^*}{\partial t^*} = \frac{1}{r^{*2}}\frac{\partial}{\partial r^*}\left(r^{*2}\epsilon^2\frac{\partial C_A^*}{\partial r^*}\right) - h^2(1 - \gamma\epsilon)(1 - \epsilon)\epsilon C_A^* \tag{10}$$

$$\frac{\partial \epsilon}{\partial t^*} = q(1 - \epsilon_0)(1 - \gamma\epsilon)(1 - \epsilon)\epsilon C_A^* \tag{11}$$

where $r^* = r/R$, $C_A^* = C_A/C_{A,s}$, $h = R(k_0\rho_t S/D)^{1/2}$ = Thiele modulus, $t^* = k_0\rho_t St$, $q = C_{A,s}/C_c^0$ and $C_c/C_c^0 = (1 - \epsilon)/(1 - \epsilon_0)$. The boundary conditions are:

$$C_A^* = 1 \text{ at } r^* = 1 \text{ and } \frac{\partial C_A^*}{\partial r^*} = 0 \text{ at } r^* = 0. \tag{12}$$

The accumulation term in Eq. 10 is much smaller than other terms by order of magnitude (Bischoff, 1963). Therefore

$$0 = \frac{1}{r^{*2}}\frac{\partial}{\partial r^*}\left(r^{*2}\epsilon^2\frac{\partial C_A^*}{\partial r^*}\right) - h^2(1 - \gamma\epsilon)(1 - \epsilon)\epsilon C_A^* \tag{13}$$

$$\frac{\partial \epsilon}{\partial \tau^*} = (1 - \epsilon_0)(1 - \gamma\epsilon)(1 - \epsilon)\epsilon C_A^* \tag{14}$$

where $\tau^* = qt^*$.

Equations 13 and 14 contain only two parameters, h and γ, each of which, in principle, can be estimated by independent means. (One can also use these parameters empirically to fit existing data sets.) The case of $\gamma = 0$ arises when the reaction rate constant is not a function of conversion. In this important special case only one free parameter, h, is required to fit isothermal gasification data. Equations 13 and 14 are coupled nonlinear partial differential equations and quite difficult to solve. Even numerical routines are sometimes difficultt to formulate, when one has a "wavelike" form of porosity distribution or when h is very large (e.g., $h > 50$). However the numerical solution is not very appealing for many engineering purposes, and one would like an analytic or semi-analytic solution to use whenever possible.

Analytic or Approximate Solutions

Various methods of obtaining semi-analytic or approximate solutions in the asymptotic regions of high and low Thiele moduli will be presented.

Reaction Controlling Case. If the classic Thiele modulus is small (say, $h < 1$), the concentration of gaseous reactant is essentially constant and equals the outer surface concentration, $C_{A,s}$. Then the problem can be formulated by setting $C_A^* = 1$ in Eq. 14.

$$\frac{\partial \epsilon}{\partial \tau^*} = (1 - \epsilon_0)(1 - \gamma\epsilon)(1 - \epsilon)\epsilon \tag{15}$$

Integration of Eq. 15 by separation of variables yields the following equation which relates the variation of local porosity with time:

$$\frac{\gamma}{(1 - \gamma)(1 - \epsilon_0)}\ln\frac{1 - \gamma\epsilon}{1 - \gamma\epsilon_0} - \frac{1}{(1 - \gamma)(1 - \epsilon_0)} \times \ln\frac{1 - \epsilon}{1 - \epsilon_0} + \frac{1}{(1 - \epsilon_0)}\ln\left(\frac{\epsilon}{\epsilon_0}\right) = \tau^* \tag{16}$$

Rewriting Eq. 16 in terms of local conversion, one obtains

$$\frac{\gamma}{(1 - \gamma)(1 - \epsilon_0)}\ln\frac{1 - \gamma + \gamma(1 - \epsilon_0)(1 - x)}{1 - \gamma\epsilon_0} - \frac{1}{(1 - \gamma)(1 - \epsilon_0)}\ln(1 - x) + \frac{1}{(1 - \epsilon_0)}\ln\frac{1 - (1 - \epsilon_0)(1 - x)}{\epsilon_0} = \tau^* \tag{17}$$

If the initial porosity distribution is uniform, then the local carbon conversion is always equal to the overall carbon conversion, i.e., $x = X$. Note the simplification in Eq. 17 when $\gamma = 0$.

Experimental results sometimes show the overall reaction rate reaches a maximum value after which it decreases. The present model allows the possibility of such a maximum. The maximum and minimum locations are obtained from Eq. 15 by using the condition $d/dX(dX/d\tau^*) = 0$. The maximum, if it exists, is at

$$X_{MX} = \frac{(1 - 2\gamma) - \sqrt{1 - \gamma + \gamma^2}}{3\gamma(1 - \epsilon_0)} + 1 \tag{18}$$

and minimum, if it exists, occurs at

$$X_{MN} = \frac{(1 - 2\gamma) + \sqrt{1 - \gamma + \gamma^2}}{3\gamma(1 - \epsilon_0)} + 1 \tag{19}$$

It should be noted that Eqs. 18 and 19 are applicable only under the restrictions:

$$0 \le x_{MX}, X_{MN} \le 1;\quad 0 < 1 - \gamma\epsilon_0;\quad 0 < 1 - \epsilon_0;\quad 0 < \gamma, \epsilon_0 \tag{20}$$

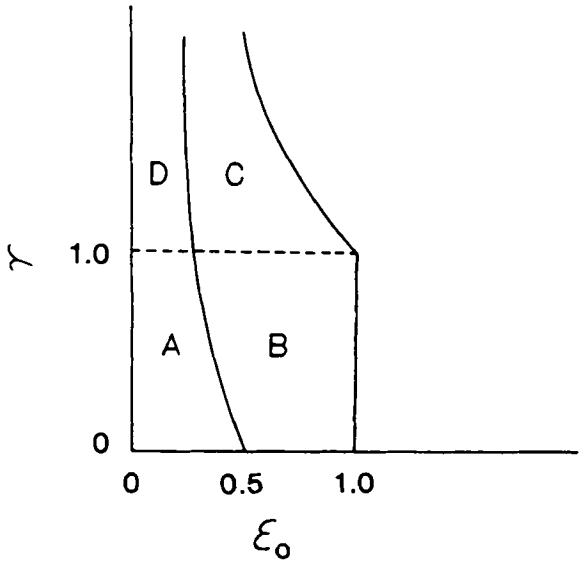

Figure 1. Regions where extrema in gasification rate can occur: A, Maximum; B, No Extremum; C, Minimum; D, Minimum and Maximum. (h = 0).

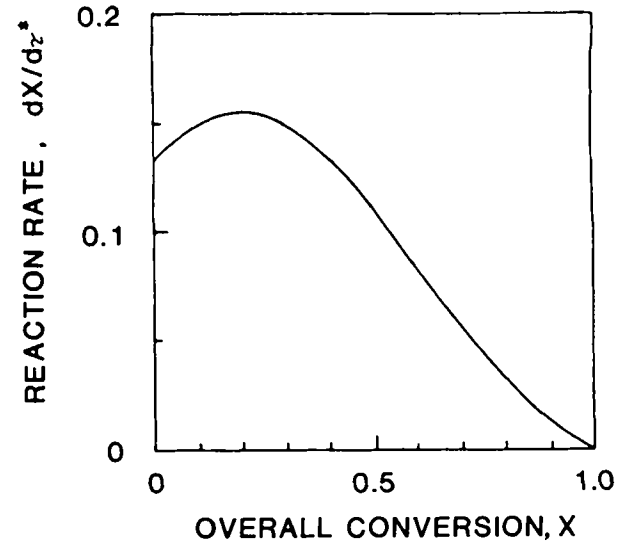

Figure 2. Calculated reaction rate vs. conversion for situation where rate reaches a maximum; h = 0, ϵ_0 = 0.2 and γ = 0.9.

The criteria for the existence of extrema are synthesized in the $\gamma - \epsilon_0$ diagram (Figure 1). Figure 1 shows a wide region where minima in rates can occur. However, in fact, minima are not observed because γ is normally less than 1, i.e, the intrinsic reaction rate decreases with increasing conversion. The maximum occurring region in the figure is where one sees the maxima in real experiments with low porosity coal char. Figure 2 shows a typical example of the occurrence of a maximum in the reaction rate. The values of γ and ϵ_0 for this example, i.e., $\gamma = 0.9$ and $\epsilon_0 = 0.2$, are in region A of Figure 1.

The maximum in rate arises from the competing effects of conversion on rate constant, density and surface area, which give rise to the $(1 - \gamma\epsilon)$, $(1 - \epsilon)$ and ϵ terms respectively in Eq. 15. Note that for $\gamma = 0$ the latter two terms can by themselves give rise to a maximum.

Diffusion Controlling Case. If the classic Thiele modulus is large (say, $h > 5$), then there exists a large concentration gradient of gaseous reactant inside the particle. As a result, the reaction is faster near the surface than near the center. The pseudosteady-state approximation is also valid for this case. The initial concentration profile of gaseous reactant can be obtained from equation (13) for a uniform initial porosity distribution:

$$C_A^*(0,r^*) = \frac{1}{r^*}\frac{\sinh \phi_0 r^*}{\sinh \phi_0} \tag{21}$$

where ϕ_0 = a modified Thiele modulus = $h\{(1 - \gamma\epsilon_0)(1 - \epsilon_0)/\epsilon_0\}^{1/2}$.

By combining Eqs. 21 and 14, a short-time solution for porosity development can be obtained. Obviously, it is not a good approximation for the long-time case, because the porosity profile changes as time proceeds. However, it seems tempting to seek an asymptotic form of the solution to Eq. 13 in the following way:

$$C_A^* = \frac{\sinh \psi r^*}{r^* \sinh \psi} \tag{22}$$

where ψ is an unknown function of r^* and t^*. One asymptotic solution can be obtained by putting

$$\psi = h\{(1 - \gamma\epsilon)(1 - \epsilon)/\epsilon\}^{1/2}. \tag{23}$$

In this case, an updated porosity function, $\epsilon(r^*,t^*)$ is used to calculate the concentration profile from Eqs. 22 and 23. It should be noted here that the selection of ψ is open and an empirical procedure is also feasible. Equation 22 along with Eq. 23 is also a good approximation for the intermediate region, where both reaction and diffusion are equally important.

Power Series Solution. The power series solution technique can be readily applied to this problem; however, much algebraic manipulation is required to attain the same order of accuracy as the approximate solution given by Eqs. 22 and 23. Further detail can be found in the original work by Lee (1980).

Numerical Solution. The Crank-Nicolson method can be applied to Eqs. 13 and 14 with a slight modification. Taking central differences in space and backward differences in time, one can reduce the two differential equations to a system of algebraic equations in terms of $C_{k,i}$ and $\epsilon_{k,i}(k = 1,2,\ldots,m; i = 1,2,\ldots,n)$. $C_{k,i}$ and $\epsilon_{k,i}$ represent the gaseous concentration and the porosity at ith mesh in radius and kth time stage.

As the classic Thiele modulus gets larger, the system becomes more stiff because its characteristic value tends to increase. Consequently, the numerical routine requires a finer mesh size. If the classic Thiele modulus is greater than 50, then this numerical routine requires a very fine mesh. However, an asymptotic solution can be rather easily obtained because the situation is nearly the same as that of the unreacted shrinking core model.

Figure 3 shows the initial gas concentration profile for various Thiele moduli at $\epsilon_0 = 0.3$ and $\gamma = 0.4$. The curves were obtained numerically from Eq. 13. Figures 4a and 4b show the instantaneous gaseous concentration profile and local porosity profile for a dif-

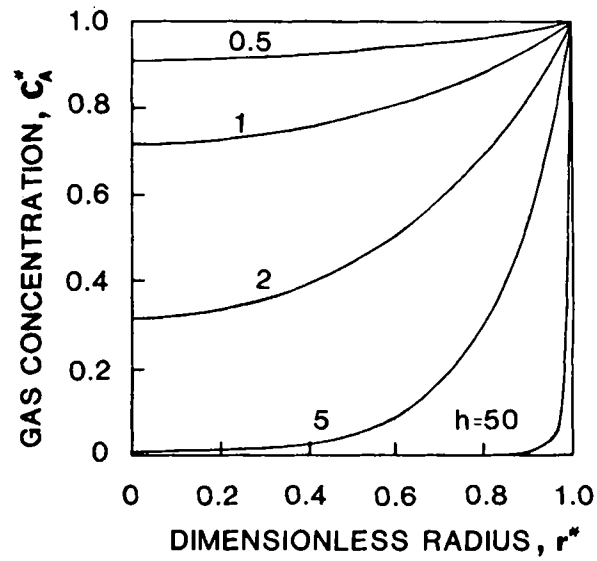

Figure 3. The initial gas concentration profile for various Thiele moduli at ϵ_0 = 0.3 and γ = 0.4. (Isothermal Solution).

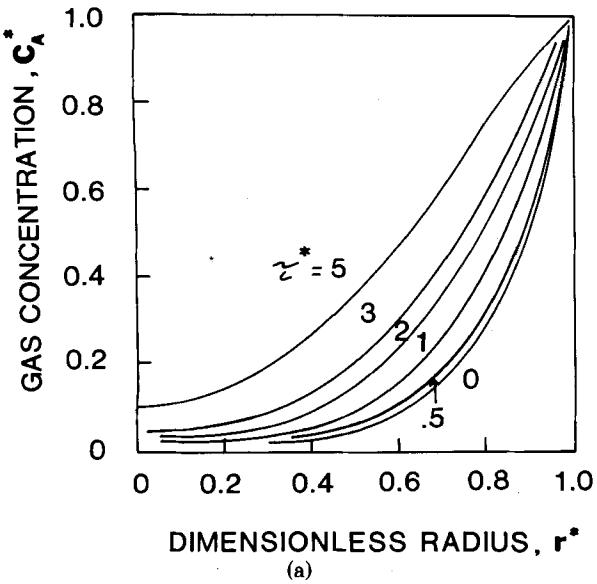

(a)

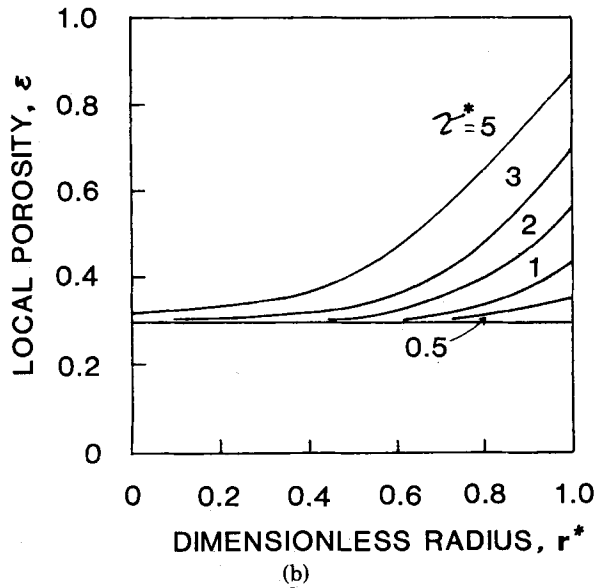

(b)

Figure 4. Isothermal Solution (h = 5, ϵ_0 = 0.3 and γ = 0.4). (a) Gas concentration vs. particle radius; (b) Local porosity vs. particle radius

fusion-limited process, respectively. A comparison between the approximate solution, integrated using Eqs. 22 and 23, and the numerical solution is made for the case of $h = 5$, $\epsilon_0 = 0.3$, $\gamma = 0.4$ and $\tau^* = 5$. As shown in Figure 5, Eq. 22 along with Eq. 23 provides a good approximation for the instantaneous gas concentration profile. At $\tau^* = 0$, these two solutions are, of course, identical.

Existence of A Universal Curve. Recent work by Mahajan et al. (1978) showed that the overall conversion curves, $X(t)$, for different temperatures, pressures, reactant gases and chars approximately reduced to a single universal curve when plotted against the dimensionless time $t/t_{0.5}$. The half conversion time $t_{0.5}$ is defined as the value of t at $X = 0.5$, i.e., $X(t_{0.5}) = 0.5$. For air at 1.013 $\times 10^5$ Pa and 678 K, CO_2 at 1.013 $\times 10^5$ Pa and 1,173 K, steam at 2.2286 $\times 10^3$ Pa and 1,183 K and H_2 at 2.7554 $\times 10^6$ Pa and 1,253 K, all conversion data were successfully correlated by

$$X = 0.37(t/t_{0.5}) + 0.28(t/t_{0.5})^2 - 0.15(t/t_{0.5})^3 \qquad (24)$$

An interesting question which may be asked here is under what conditions, if any, the present model predicts the existence of this kind of curve.

The overall conversion $X(\tau^*)$, calculated from the present model (Eqs. 13 and 14) is plotted against the dimensionless time $\tau^*/\tau^*_{0.5}$

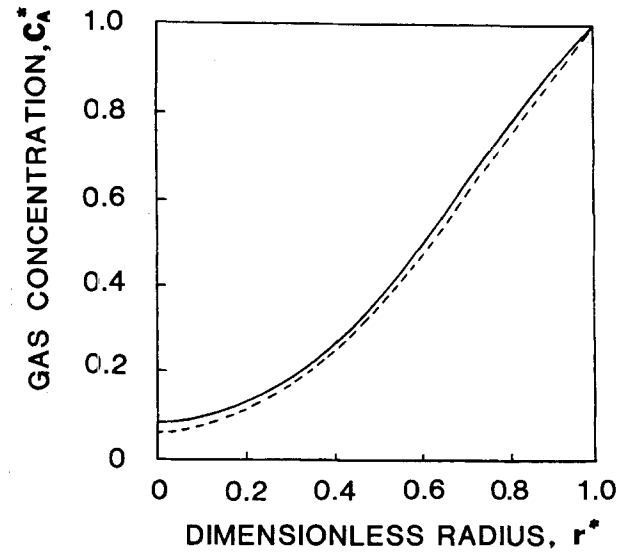

Figure 5. A comparison between the exact solution and the approximate solution (equations (22) and (23)); h = 5, ϵ_0 = 0.3, γ = 0.4 and τ^* = 5. —, Exact Solution: - - -, Approximate Solution.

for the various Thiele moduli in Figure 6. For $h \leq 5$, the curves can be reasonably approximated by a single curve.

If the gasification rate is controlled solely by the surface reaction and the parameter γ is the same for different gases, then the model predicts there exists exactly one master curve, $X(\tau^*/\tau^*_{0.5})$. This universal curve can be obtained by dividing Eq. 17 by the following equation that is also derived from Eq. 17:

$$\frac{\gamma}{(1-\gamma)(1-\epsilon_0)} ln \frac{1-\gamma+0.5\gamma(1-\epsilon_0)}{1-\gamma\epsilon_0} + \frac{ln\,2}{(1-\gamma)(1-\epsilon_0)} + \frac{1}{(1-\gamma)(1-\epsilon_0)} ln \frac{0.5(1+\epsilon_0)}{\epsilon_0} = \tau^*_{0.5} \qquad (25)$$

Thus, the final form of the universal curve is:

$$\tau^*/\tau^*_{0.5} = g(X;\gamma,\epsilon_0) \qquad (26)$$

Since the initial porosity ϵ_0 is a known (measured) quantity, the only free parameter for the model in the reaction-controlling regime is γ. Recall that $\tau^*_{0.5}$ is a unique function of γ, as shown in Eq. 25. If γ is equal to zero, then ϵ or X is only a function of $\tau^*/\tau^*_{0.5}$. The overall conversion X of Eq. 26 was plotted against $\tau^*/\tau^*_{0.5}$ for

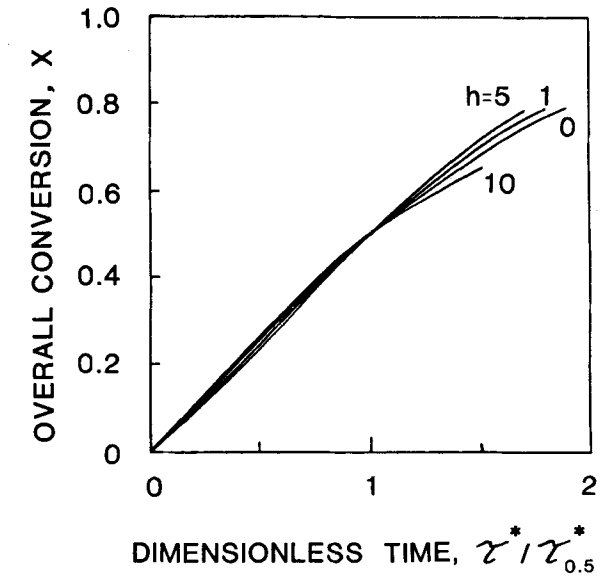

Figure 6. The X vs. $\tau^*/\tau^*_{0.5}$ curves for various Thiele moduli; ϵ_0 = 0.3 and γ = 0.4.

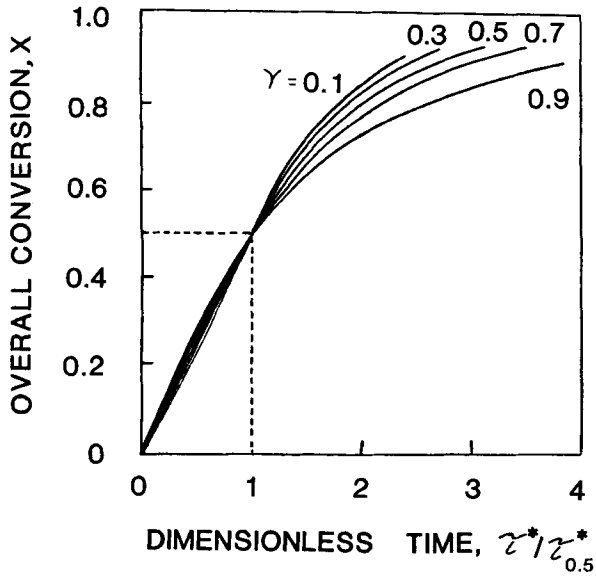

Figure 7. The X vs. $\tau^*/\tau^*_{0.5}$ curves for parametric values of γ; h = 0 and $\epsilon_0 = 0.3$.

parametric values of γ and shown in Figure 7. The value of parameter γ for a certain char gasification reaction can be easily selected by the least square technique. The correlation given by Eq. 24 merely corresponds to the $\gamma = 0.7$ case of the present model.

In the diffusion controlling regime, the overall conversion vs. dimensionless time curves, in general, cannot be closely represented by a single universal curve. As the Thiele modulus h increases, less of the particle volume becomes accessible to high gas concentrations. The evolution of porosity, surface area and gaseous concentration will differ depending on the value of h. It should be noted that the conditions which yielded the correlation (Eq. 24), are in fact in the reaction-controlling region.

A universal curve will exist when the system is in the reaction rate controlling regime and when the evolution of porosity, surface area and reactivity are the same. Only the reactivity is allowed to evolve differently depending on the value of γ. Once the value of γ is set, then $\tau^*_{0.5}$ is automatically fixed and is related to the surface reaction rate constant by:

$$\tau^*_{0.5} = (k_0\rho_t S)(C_{A,s}/C^0_c)t_{0.5} \tag{27}$$

where $C_{A,s}/C^0_c$ can be calculated from the external condition such as temperature, pressure and solid density. Therefore, $t_{0.5}$ is just another way of reporting the surface reaction rate constant in the reaction rate controlling regime.

NONISOTHERMAL PARTICLE MODEL

In the previous section, the isothermal assumption eliminated the energy equation and considerably simplified the analysis. However, if the rate of evolution of the heat of reaction is sufficiently large, a nonnegligible temperature gradient may exist.

Consider a spherical particle reacting with a gas whose bulk concentration and temperature are $C_{A,s}$ and T_b, respectively. If we again assume there is no mass and heat transfer resistance in the gas film, then the differential energy balance is:

$$\frac{\partial \rho_p c T}{\partial t} = \nabla \cdot (k_e \nabla T) + (-\Delta H_c)(r_c) \tag{28}$$

The gas-phase heat capacity was neglected in Eq. 28. Initial and boundary conditions are:

$$C_c = C^0_c, \quad T = T_i; \quad \text{at } t = 0 \tag{29a}$$

$$C_A = C_{A,s}, \quad T = T_b; \quad \text{at } r = R \tag{29b}$$

$$\nabla C_A = 0, \quad \nabla T = 0; \quad \text{at } r = 0 \tag{29c}$$

Boundary conditions (Eq. 29b) are direct consequences of the assumption that there is no heat and mass transfer resistance in the boundary layer.

An *a priori* assumption for the effective thermal conductivity is needed. By analogy to the effective diffusivity

$$k_e = k_c(1 - \epsilon)^2 \tag{30}$$

Substituting Eqs. 6 and 30 into Eq. 28, one obtains a final form of the energy balance. Then, the complete formulation for the nonisothermal particle is:

$$\frac{\partial \epsilon C_A}{\partial t} = \frac{1}{r^2}\frac{\partial}{\partial r}\left(r^2\epsilon^2 D \frac{\partial C_A}{\partial r}\right) - r_A \tag{31}$$

$$\rho_t c \frac{\partial (1-\epsilon)T}{\partial t} = \frac{1}{r^2}\frac{\partial}{\partial r}\left(r^2(1-\epsilon)^2 k_c \frac{\partial T}{\partial r}\right) + (-\Delta H_c)r_c \tag{32}$$

$$-r_A = -r_c = A\rho_t S e^{-E_0/RT}(1 - \gamma\epsilon)(1 - \epsilon)\epsilon C_A \tag{33}$$

where A is the frequency factor for the rate constant. The pseudosteady-state approximation can be applied to Eqs. 31 and 32, making the left hand sides of the equation vanish.

Approximate Solution and Isothermality Criteria

Inspection of Eqs. 31 and 32 shows their similarity. By using the pseudosteady-state approximation and eliminating $-r_c$ (or $-r_A$) from the two equations, one obtains:

$$\frac{1}{r^2}\frac{\partial}{\partial r}\left\{r^2\left(\epsilon^2 D \frac{\partial C_A}{\partial r} + \frac{(1-\epsilon)^2 k_c}{(-\Delta H_c)}\frac{\partial T}{\partial r}\right)\right\} = 0 \tag{34}$$

By applying boundary conditions (Eq. 29c),

$$\frac{\partial T}{\partial r} = -\frac{\epsilon^2 D(-\Delta H_c)}{(1-\epsilon)^2 k_c}\frac{\partial C_A}{\partial r} \tag{35}$$

Equation 35 can be integrated easily by assuming $\epsilon^2/(1-\epsilon)^2$ is a weak function of radius. This assumption is exact at the initial time and valid at low conversions. Then, the integrated equation is given by:

$$T_b - T = -\frac{\epsilon_s^2 D(-\Delta H_c)}{(1-\epsilon_s)^2 k_c}(C_{A,s} - C_A) \tag{36}$$

Assume the reaction is endothermic. Since $C_{A,s} \geq C_A \geq 0$ always, the temperature bounds inside the char particle are:

$$T_b \geq T \geq T_b + \frac{\epsilon_s^2 D(-\Delta H_c)C_{A,s}}{(1-\epsilon_s)^2 k_c} \tag{37}$$

If the reaction is exothermic, the upper and lower bounds for the temperature are:

$$T_b \leq T \leq T_b + \frac{\epsilon_s^2 D(-\Delta H_c)C_{A,s}}{(1-\epsilon_s)^2 k_c} \tag{38}$$

One may derive an isothermality criterion for the reacting char particle by casting Eq. 36 into dimensionless form:

$$T^* - 1 = \frac{\epsilon_s^2 D(-\Delta H_c)C_{A,s}}{(1-\epsilon_s)^2 k_c T_b}(1 - C^*_A) \equiv \alpha_T(1 - C^*_A) \tag{39}$$

Similar expressions to Eq. 39 can be found elsewhere (Aris, 1969). Numerical solutions of Eqs. 31–33, which will be discussed later, show that isothermal conditions may be assumed to good accuracy for:

$$|\alpha_T| < 0.07 \quad \text{for} \quad h < 1 \tag{40a}$$

$$|\alpha_T| < 0.03 \quad \text{for} \quad 2 < h < 3 \tag{40b}$$

$$|\alpha_T| < 0.01 \quad \text{for} \quad h > 5 \tag{40c}$$

These criteria were based on a maximum 10 K difference between the bulk and the lowest inside temperatures at T_b = 1,200 K.

Numerical Solution

The energy balance equation (Eq. 32) is highly nonlinear in temperature. The Crank-Nicolson method with quasilinearization

was used to obtain complete solutions for gaseous concentration, temperature profile and local conversion.

Parameters for the nonisothermal particle model are:

$$h^2 = \frac{R^2 A \rho_t S e^{-E_0/RT_b}}{D}, \quad \alpha_T = \frac{\epsilon^2 D(-\Delta H_c) C_{A,s}}{(1-\epsilon)^2 k_c T_b},$$

$$\delta = \frac{E_0}{RT_b} \text{ and } \gamma.$$

The above defining equations are easily obtained by casting Eq. 32 into a dimensionless form.

In Figure 8a, the time variation of gaseous concentration profile is shown for a nonisothermal example ($h = 5$, $\epsilon_0 = 0.3$, $\gamma = 0.4$, $\alpha_T = -0.5$ and $\delta = 20$) and compared with the corresponding isothermal case ($h = 5$, $\epsilon_0 = 0.3$, $\gamma = 0.4$). As the reaction proceeds, the gaseous concentration profile for the nonisothermal case becomes closer to that of a reaction-controlling case, i.e., the concentration is virtually constant across the particle. This is due to the slow reaction rate at the inner core, where the temperature is lower than at the outer surface. Figure 8b shows the variation of temperature profile as a function of the dimensionless time (τ^*) when $h = 5$, $\epsilon_0 = 0.3$, $\gamma = 0.4$, $\alpha_T = -0.5$ and $\delta = 20$. The local porosity vs. radius curves at the same conditions are shown in Figure 8c. The porosity profile for the nonisothermal case is even sharper than that for the isothermal case. This arises from the relatively rapid rate of chemical reaction at the hot outer surface and the slow reaction rate at the cool inner core.

For a typical char-CO_2 reaction, $\epsilon_0 = 0.4$, $\Delta H = 1.7166 \times 10^2$ kJ/mol, $T_b = 1{,}250$ K, $k_c(1-\epsilon)^2 = 1.6747$ J/m·s·K (Badzioch et al., 1964), $D = 5 \times 10^{-6}$ m^2/s (Knudsen diffusion corresponding to the pore diameter of 20 nm) and $C_{A,s} = 70$ mol/m^3 (a partial pressure of 6.8948×10^2 kPa), the calculated value of $|\alpha_T|$ is 0.005 and h is much smaller than unity for 14 × 18 mesh size sample. As expected from the criteria of Eq. 40, numerical results show that the temperature gradient inside the particle is negligible for $|\alpha_T| = 0.005$ and $\delta = 23$. If the porosity value is abnormally high and the diffusivity is a comparatively large number, then $|\alpha_T|$ would be greater. For most endothermic char reactions at practical fixed-bed operating conditions, the isothermal assumption is valid, i.e., the value of $|\alpha_T|$ is fairly small regardless of h. Therefore, an isothermal assumption can be safely made for most endothermic char reactions.

For exothermic reactions, the intrinsic reaction rate is faster at the inner core than at the exterior surface of the particle, due to the exothermic heat of reaction. The hydrogasification is an exothermic reaction; however, relatively slow gasification rates and small values of $|\alpha_T|$ (order of 0.01) at most fixed-bed operating conditions (1,100–1,300 K) make the isothermality assumption still valid.

EXPERIMENTAL DATA ANALYSIS

The carbon dioxide gasification of the Montana Rosebud Char and the Illinois No. 6 Char was investigated at various reaction temperatures to test the model. A unique experimental system, the "Hanging Reactor Thermobalance," was used for this purpose. A detailed description of this device has been given elsewhere (Gardner et al., 1980; Angus et al., 1980).

Surface Area and Porosity Determination

The densities of Montana Rosebud and Illinois No. 6 chars at various conversions were determined by helium displacement and mercury penetration. The helium and mercury densities are used to calculate the total void volume of the particle, which in turn determines the overall porosity of the particle, as shown in Table 1. Mercury density was measured in a mercury porosimeter at 101.3 kPa pressure. Pores with radii smaller than 15 μm are not penetrated at that pressure. Taking the helium density as the true density of the solid matrix and the mercury density as the bulk density, the following relationships can be used:

$$v_g = \rho_p^{-1} - \rho_t^{-1} \tag{41}$$

$$\epsilon = 1 - \rho_p/\rho_t \tag{42}$$

where v_g denotes the pore volume of particle.

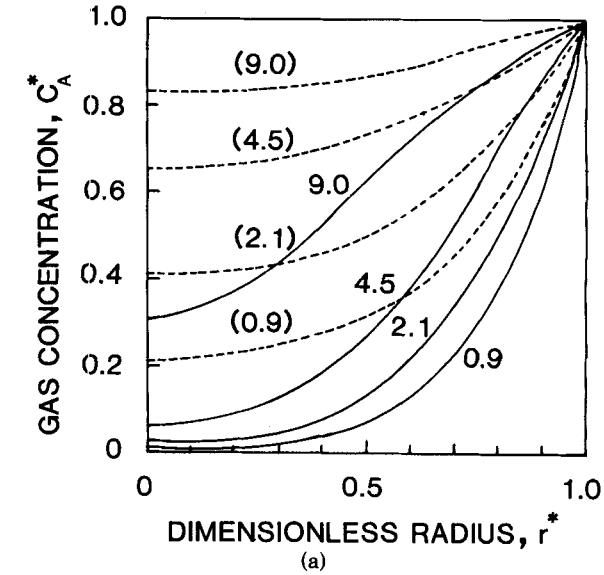

(a)

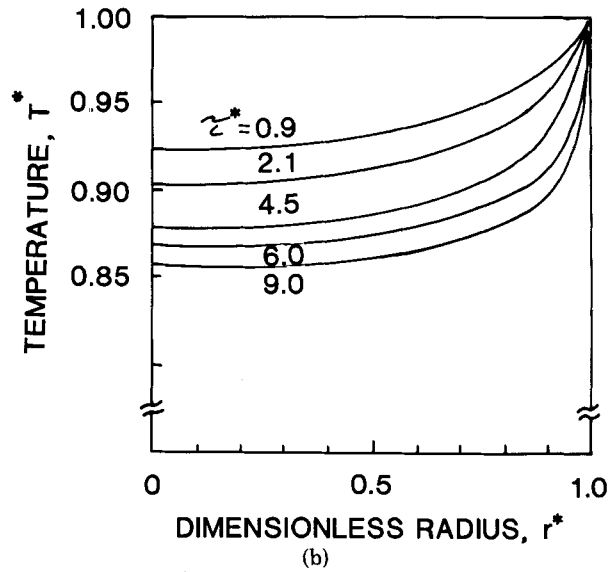

(b)

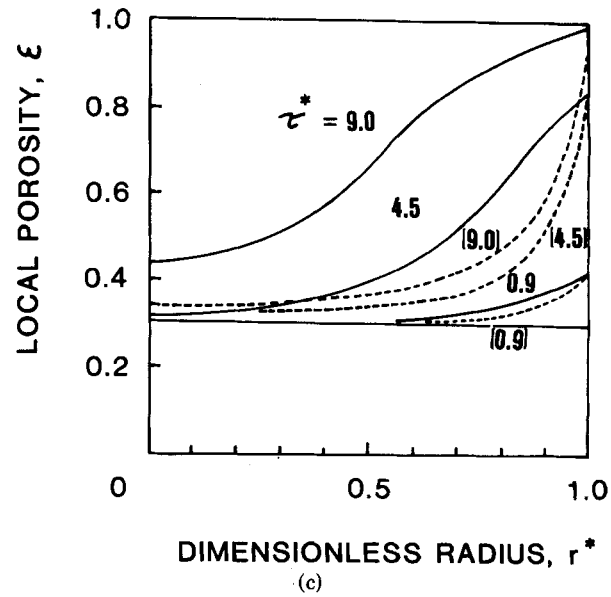

(c)

Figure 8. Time variation of various profiles for h = 5, $\epsilon_0 = 0.3$ and $\gamma = 0.4$. (a) Gas concentration profile: —, Isothermal; - - -, Nonisothermal ($\alpha_T = -0.5$ and $\delta = 20$). (b) Temperature profile for nonisothermal case. (c) Local porosity profile: —, Isothermal; - - -, Nonisothermal.

TABLE 1. MORPHOLOGICAL DATA OF CHAR SAMPLES USED

	Helium Density Mg/m³	Mercury Density Mg/m³	Void Volume m³/Mg	Porosity	Specific Surface Area, m²/kg
Montana Rosebud Char					
Raw Sample	1.718	0.8850	0.5479	0.4849	3.96×10^5
30% Conversion	2.030	0.8748	0.6505	0.5691	4.30×10^5
50% Conversion	2.111	0.8878	0.6527	0.5795	4.26×10^5
70% Conversion	2.166	0.6648	1.0425	0.6951	4.61×10^5
100% Conversion	2.247	—	—	—	—
Illinois No. 6 Char					
Raw Sample	1.729	0.7876	0.6913	0.5445	2.51×10^5
40% Conversion	2.090	0.7336	0.8847	0.6490	3.29×10^5

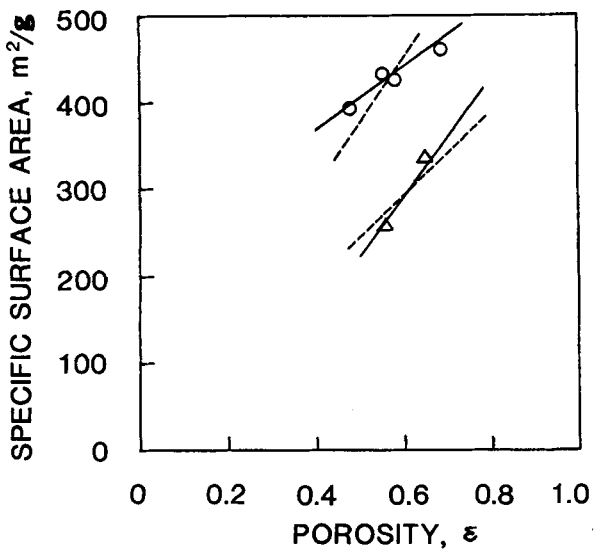

Figure 9. The surface area vs. porosity curves: O, Montana Rosebud; △, Illinois No. 6; - - -, Sg = Sε.

The specific surface areas for the same samples were measured using CO_2 adsorption, also shown in Table 1. Figure 9 shows how the specific surface area increases with porosity for Montana Rosebud and Illinois No. 6 chars. Even though it was clearly impossible to obtain a universal correlation regardless of char type, an approximately linear functionality between the specific surface area and porosity can be assumed, as is shown in Figure 9. The empirical equation (Eq. 5) appears to be a reasonable approximation in the range of moderate conversions (Walker et al., 1959). Values of S, defined in Eq. 5, were determined by the least square method as 745 (m^2/g) for Montana Rosebud char and 490 (m^2/g) for Illinois No. 6 char.

Experimental Determination of Reaction Order

The experimental fractional conversion of the coal char is defined in two different ways:

$$(i)\ \text{Ash free basis:}\quad \tilde{X} = 1 - \frac{(M_s)_t - M_a}{(M_s)_0 - M_a} \tag{43}$$

$$(ii)\ \text{Dry mineral matter free basis:}\quad X = \frac{(M_s)_t - M_v - M_a}{(M_s)_0 - M_v - M_a} \tag{44}$$

The above two definitions of fractional conversion will be used in the rest of data analysis.

The 35 × 60 mesh sieve fractions of Montana Rosebud char were gasified with CO_2 at various conditions in the reaction rate controlling regime. The partial pressure of CO_2 was suddenly changed to another pressure at intermediate conversion. Comparing the reaction rates immediately before and after the step change in pressure, the reaction order with respect to the carbon dioxide concentration at high pressure (350–2,760 KPa) was obtained as close to *one*, as reported in Table 2. The results are in good agreement with those by Blackwood and Ingeme (1960). More detail can be found in the work by Lee (1980).

Intrinsic Reaction Rate

The 35 × 60 mesh sieve fractions of Montana Rosebud char were gasified with carbon dioxide at 1,083, 1,123, 1,163, 1,193 K and at 1,380 kPa. The fractional conversion vs. time curves can be found in Figure 10a. The average particle radius can be obtained by assuming spherical particles and is approximately 0.000125 m.

The molecular diffusion coefficients for the CO_2-CO binary gas system, $D_{CO_2\text{-}CO}$, can be calculated using the Enskog-Chapman equation as a function of both temperature and pressure. In the molecular diffusivity calculation, only the bulk diffusion in the macropores is considered. For diffusion occurring in micro and transitional pores predominantly by Knudsen flow, the Knudsen diffusivity can be approximated from the Satterfield correlation assuming cylindrical pores:

$$D_K = 19{,}400 \frac{1}{\tau_m S_g \rho_p} \sqrt{T/M} \tag{45}$$

Again, the tortuosity is assumed to be equal to the reciprocal of porosity. The molecular, Knudsen and overall diffusivities were calculated using the Enskog-Chapman equation, Satterfield correlation and resistance relation ($D^{-1} = D_f^{-1} + D_K^{-1}$), respectively and are shown in Table 3.

Previously, the dimensionless time was defined in Eq. 14 and rewritten as:

$$\tau^* = \left(\frac{C_{A,s}}{C_c^0}\right)(k_0 \rho_t S)t = \left(\frac{C_{A,s}}{C_c^0}\right)\left(\frac{h^2 D}{R^2}\right)t \tag{46}$$

The procedure for determining the reaction rate constant is essentially based on the least square method. In Eq. 46, values of $C_{A,s}$, C_c^0, R and D are obtained from measurements or calculated from correlations. Therefore, each gasification condition generates one defining equation relating the dimensionless time with real time. For example, one obtains the following defining relations for carbon dioxide gasification reactions at various temperatures and 1380 kPa.

$$\tau^* = 0.21951\, h^2 t \text{ at } 1{,}083 \text{ K} \tag{47a}$$

$$\tau^* = 0.21728\, h^2 t \text{ at } 1{,}123 \text{ K} \tag{47b}$$

TABLE 2. DETERMINATION OF REACTION ORDER FOR CO_2 GASIFICATION OF MONTANA ROSEBUD CHAR

Run	T,K	$\hat{X}_s$	P_1, kPa	P_2, kPa	$\left(\frac{d\hat{x}}{dt}\right)_{P_1}$, s^{-1}	$\left(\frac{d\hat{x}}{dt}\right)_{P_2}$, s^{-1}	n
a	1,123	0.43	1,380	2,070	7.30×10^{-4}	1.108×10^{-3}	1.03
b	1,163	0.34	690	345	6.50×10^{-4}	3.00×10^{-4}	1.12
c	1,183	0.53	1,725	862.5	4.26×10^{-4}	2.02×10^{-4}	1.08

X_s = conversion at which pressure is changed suddenly
P_1 = pressure before the step change
P_2 = pressure after the step change

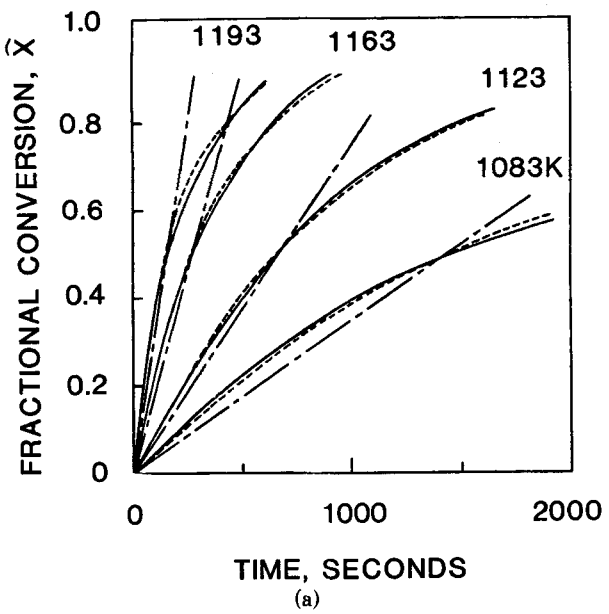

(a)

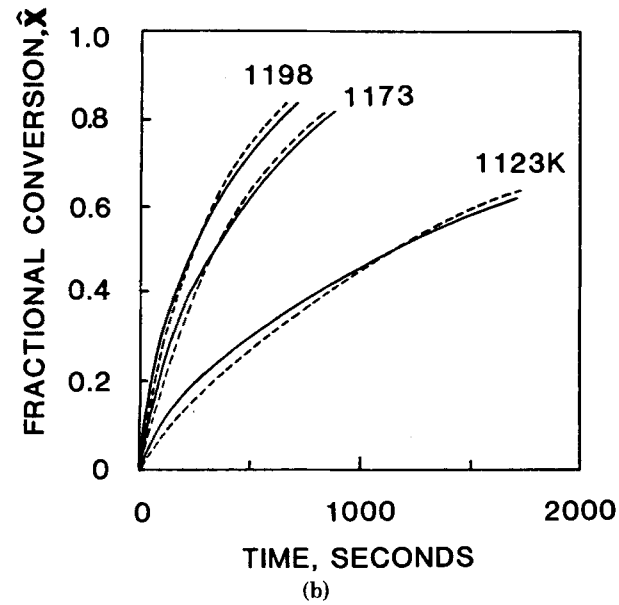

(b)

Figure 10. Fractional conversion vs. time curves for CO_2 gasification of chars. (a) Montana Rosebud char: ——, Experiments; - - -, This model; -·-, Progressive conversion model. (b) Illinois No. 6 char: ——, Experiments; - - -, This model.

$$\tau^* = 0.21485\, h^2 t \text{ at } 1{,}163 \text{ K} \tag{47c}$$

$$\tau^* = 0.21339\, h^2 t \text{ at } 1{,}193 \text{ K} \tag{47d}$$

By plotting the experimental conversion data ($\hat{X}$) against the dimensionless time ($t/t_{0.5}$) and comparing these curves with the theoretical X vs. $\tau^*/\tau^*_{0.5}$ curves at an assumed Thiele modulus (h), one can obtain the value of γ using the least square method. An updated value of h is calculated by using Eq. 47 at the perfect fitting point, i.e., $X = \hat{X} = 0.5$. If the assumed h and the calculated h are equal, then the iterative calculation stops; if not, the procedure is repeated with the updated value of h.

If the reaction rate is controlled solely by surface reaction, then the calculation does not require the iterative procedure because there is only one solution for this case, i.e., Eq. 17. However, if the diffusional process affects the gasification rate, then the iterative procedure is required.

The intrinsic reaction rate constants for carbon dioxide gasification of Montana Rosebud char were calculated by analyzing the previous four runs as described above. The predictions of fractional conversion (X) vs. time were plotted at the four different temperatures and compared with the experimental data and to the progressive conversion model (Ishida and Wen, 1968) in Figure 10a.

Since the Arrhenius-type temperature dependence is assumed in the model, the activation energy can be obtained by plotting (lnk_0) against ($1/T$). The calculated activation energy E_0 for CO_2 gasification of Montana Rosebud char is 2.495×10^2 kJ/mol. The dependence of the activation energy upon the fractional conversion is obtained from Eqs. 7 and 8 as:

$$E = (2.495 + 0.065\epsilon) \times 10^2 \text{ kJ/mol}$$

$$= (2.529 + 0.033X) \times 10^2 \text{ kJ/mol} \tag{48}$$

The average activation energy from the present study is found to lie between the literature values of $2.261\text{–}2.847 \times 10^2$ kJ/mol. Accordingly, the rate constant can be represented by an Arrehenius-type equation as follows:

$$k_0 = 687.54 \exp(-2.495 \times 10^2/RT)(\text{m/s}) \tag{49}$$

As shown in Table 4, the chemical reaction controls the process at temperatures up to 1,193 K at 1380 kPa. At higher temperatures, however, diffusion resistance may become appreciable. There is a critical temperature above which pore diffusion significantly limits the reaction rate for a given size particle at a fixed partial pressure of the gaseous reactant. If one uses $h > 5$ as the criterion for the onset of diffusion limitation, then the critical temperature (T_c) can be calculated using Newton's method. For example, the critical temperature is 1,516 K at $R = 0.000125$ m (approximately equivalent to 35×60 mesh), $P = 1{,}380$ kPa and $T_r = 1{,}193$ K. If the particle size is increased to $R = 0.000625$ m (approximately equivalent to 12×14 mesh), then the critical temperature is 1,300 K. Similarly, the critical radius can be defined as the radius at which pore diffusion significantly influences the rate, i.e., the radius at which $h = 5$. At $T = 1{,}123$ K and $P = 1{,}380$ kPa, the critical radius is 0.00378 m (larger than 3 mesh size sample). Many practical gasification conditions (1,073–1,273 K, 0.0001–0.002 m and 690–3,450 kPa) for various fixed bed reactors are in the reaction controlling regime.

Similarly, the carbon dioxide gasification reactions of Illinois No. 6 char were analyzed and the fractional conversion vs. time curves for 35×60 mesh are shown in Figure 10b for 1,123, 1,173, 1,198 K and 1,380 kPa of CO_2. The intrinsic reaction rate constants were calculated and are summarized in Table 5. The activation energy calculated from the slope of the Arrhenius plot is 2.389×10^2 kJ/mol. The porosity (or fractional conversion) dependence of the activation energy is:

$$E = (2.389 + 0.078\epsilon) \times 10^2 \text{ kJ/mol}$$

$$= (2.431 + 0.033X) \times 10^2 \text{ kJ/mol} \tag{50}$$

It is worthwhile to check the assumption of isothermality. Assuming $k_c(1-\epsilon)^2 = 1.6747$ J/m·s·K, α_T is found to be:

$$|\alpha_T| = 0.00872, \quad h = 0.09325; \quad \text{at } 1{,}123 \text{ K}$$

$$|\alpha_T| = 0.00829, \quad h = 0.17217; \quad \text{at } 1{,}173 \text{ K}$$

$$|\alpha_T| = 0.00810, \quad h = 0.20100; \quad \text{at } 1{,}198 \text{ K} \tag{51}$$

Therefore, according to the criteria of Eq. 40, the isothermal assumption is valid for this situation.

ANALYSIS OF LITERATURE DATA

Hydrane No. 49 char (35×60 mesh) was gasified with CO_2 by Dutta et al. (1977). Table 6 presents the data on pore characteristics.

TABLE 3. DIFFUSIVITY CALCULATIONS FOR CO_2 GASIFICATION OF MONTANA ROSEBUD CHAR

T,K	P, kPa	$D_{CO_2\text{-}CO}$, m²/s	D_k, m²/s	D, m²/s
1,083	1,380	1.046×10^{-5}	1.373×10^{-6}	1.214×10^{-6}
1,123	1,380	1.143×10^{-5}	1.398×10^{-6}	1.246×10^{-6}
1,163	1,380	1.237×10^{-5}	1.423×10^{-6}	1.276×10^{-6}
1,193	1,380	1.325×10^{-5}	1.441×10^{-6}	1.300×10^{-6}

TABLE 4. CALCULATION OF INTRINSIC REACTION RATE CONSTANTS FOR CO_2 GASIFICATION OF MONTANA ROSEBUD CHAR

T K	P kPa	h_a	γ	$t_{0.5,s}$	$t^*_{0.5}$	h_c	$k_0\rho_t S$ 1/s	k_0 m/s
1,083	1,380	0	0.6	1,450	3.475	0.1045	0.84825	6.626×10^{-10}
1,123	1,380	0	0.7	650	3.869	0.1655	2.18453	1.707×10^{-9}
1,163	1,380	0	0.7	275	3.869	0.2559	5.34761	4.176×10^{-9}
1,193	1,380	0	0.75	145	4.118	0.3648	11.07319	8.653×10^{-9}

h_a and h_c = assumed and calculated Thiele moduli, respectively

TABLE 5. CALCULATION OF INTRINSIC REACTION RATE CONSTANTS FOR CO_2 GASIFICATION OF ILLINOIS NO. 6 CHAR

T K	h_a	γ	$t_{0.5,s}$	$\tau^*_{0.5}$	$\tau^* =$	h_c	$k_o\rho_t S$ 1/s	k_0 m/s
1,123	0	0.8	1,150	4.953	$0.49527h^2t$	0.0933	1.2153	1.4345×10^{-9}
1,173	0	0.8	340	4.953	$0.49145h^2t$	0.1722	3.6991	4.3662×10^{-9}
1,198	0	0.8	250	4.953	$0.49038h^2t$	0.2010	5.9872	7.0670×10^{-9}

TABLE 6. PORE CHARACTERISTICS OF DEVOLATILIZED HYDRANE NO. 49 CHAR (DUTTA ET AL., 1977)

Properties measured by mercury porosimetry				
Net Pore Volume m^3/kg	Particle Density kg/m^3	True Density kg/m^3	Porosity	BET Method Surface Area m^2/kg
2.65×10^{-3}	0.22×10^3	1.17×10^3	0.809	1.72×10^5

The total pore surface area of the devolatilized char in the table was determined by BET nitrogen adsorption. It has been found that nitrogen at 77 K fails to reach all the micropore surface areas and some investigators such as Gan et al. (1972) and Marsh (1965) have suggested that carbon dioxide is a better adsorbate. Therefore, the surface area given should only be regarded as an approximation. The measured value of porosity seems high compared to the value given in the previous section and other literature values (Gan et al., 1972). The mechanical integrity of the pore structure remains doubtful under 34,500 kPa of mercury pressure. Nevertheless, the data appearing in the original work will be used without modification in the following analysis.

Figure 11 shows the reaction rate vs. conversion curves as a function of temperature for the Hydrane No. 49 char. A differential method can be used in this case. The present model provides the following relationship between the reaction rate and the fractional conversion (Eq. 14):

$$\frac{d\hat{X}}{d\tau^*} = \{1 - \gamma + \gamma(1 - \epsilon_0)(1 - \hat{X})\}\{(1 - \epsilon_0)(1 - \hat{X})\} \times \{1 - (1 - \epsilon_0)(1 - \hat{X})\}C^*_A \quad (52)$$

where C^*_A is approximately equal to unity for a reaction controlling case and can be approximated by a semianalytic solution for an intermediate or diffusion limiting case. The present model has only two parameters (γ and h), whereas the Dutta's model includes four parameters. The intrinsic rates are calculated and shown in Table 7. In Figure 11, Dutta's model and this model are compared. The

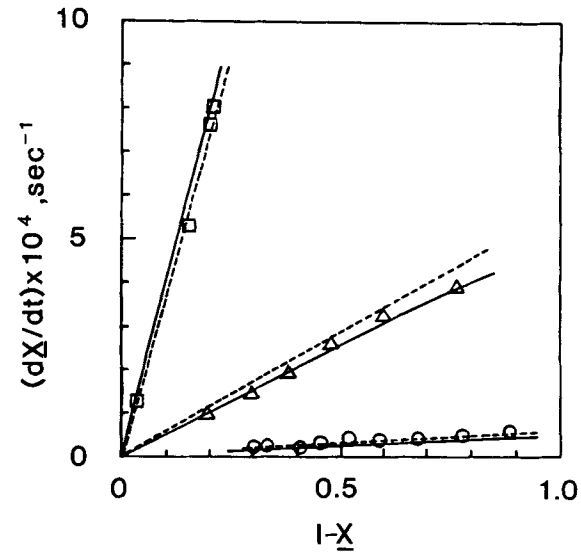

Figure 11. Reaction rate vs. conversion curves for CO_2 gasification of Hydrane No. 49 char: □, 1332 K; △, 1232 K; O, 1132 K; —, this model; - - -, Dutta's model.

sum of squares of error for the two models calculated at the data points are summarized in Table 8. It is obvious that the current two parameter model is at least as good as the Dutta's four parameter model in fitting the experimental data.

Wicke (1955) studied the reaction of spectroscopic electrode carbon at 1.013×10^4 Pa carbon dioxide pressure and obtained the following equation for the rate of the carbon-carbon dioxide reaction:

$$\text{Rate}_{C\text{-}CO_2} = 2.6 \times 10^7 \exp\{(-3.559 \pm 0.126) \times 10^2/RT\}(m/s) \quad (53)$$

At 1,123 K, the intrinsic rate constants for the char-CO_2 reaction

TABLE 7. CALCULATION OF INTRINSIC REACTION RATE CONSTANTS FOR CO_2 GASIFICATION OF HYDRANE NO. 49 CHAR

T K	P kPa	h_a	$\left(\frac{dX}{dt}\right)_{X=0.2}$ s^{-1}	$\left(\frac{dX}{d\tau^*}\right)_{X=0.2}$	γ	$k_o\rho_t S$ s^{-1}	h_c	k_o m/s
1,132	101.3	0	4.5×10^{-5}	0.108	0.2	0.52461	0.0211	2.109×10^{-9}
1,232	101.3	0	4.05×10^{-4}	0.108	0.2	5.13857	0.0641	2.066×10^{-8}
1,332	101.3	0	(7.7×10^{-4})	(0.029)	0.2	39.33665	0.1732	1.581×10^{-7}

Values in the parentheses are at $X = 0.8$.

TABLE 8. SUM OF SQUARES OF ERROR

T,K	Dutta's Model	This Model	# of Data Points
1,132	0.0177×10^{-8}	0.0229×10^{-8}	9
1,232	0.5320×10^{-8}	0.1308×10^{-8}	6
1,332	0.3920×10^{-8}	0.4716×10^{-8}	4

TABLE 9. APPROXIMATE RELATIVE RATES OF CARBON DIOXIDE GASIFICATION REACTIONS AT 1,123 K

	Intrinsic Reaction Rate Constant, m/s	Relative Rate
Montana Rosebud Char	1.7×10^{-9}	1
Illinois No. 6 Char	1.4×10^{-9}	0.82
Hydrane No. 49 Char	1.6×10^{-9}	0.94
Graphite	$0.25 \sim 3.6 \times 10^{-9}$	0.15–2.1

are compared with that for the graphite-CO_2 reaction and the results are reported in Table 9. The intrinsic rate constants (based on surface area) for various char samples are nearly the same and lie in the range of reaction rate constant for the graphite. Therefore, one can conclude that to some extent the activation energy and frequency factor for carbon dioxide gasification are independent of char type. Figure 12 shows a combined Arrhenius plot for the three chars shown in Table 9. The vertical scale was shifted arbitrarily to bring the three data sets onto the same line. This emphasizes the importance of the physical properties such as surface area and porosity in explaining differences in overall observed rates. As a result, the intrinsic reaction rate constant for carbon dioxide gasification, regardless of char type, can be represented by

$$k_0 = 760 \exp(-2.512 \times 10^2/RT)(\text{m/s}) \qquad (54)$$

in the temperature ranges of 1,073 to 1,323 K.

More literature data including some steam and hydrogen gasification runs were analyzed using the present model and the applicability of the model was further demonstrated in the work by Lee (1980).

ACKNOWLEDGEMENT

This work was supported in part by the Dept. of Energy through its research grant No. E(49-18)2368. The authors are grateful to F. Kocjancic and F. Kucera for their help in experimental measurements.

NOTATION

A = rate constant frequency factor
C_A = gaseous concentration of species A, mol/m^3
$C_{A,s}$ = bulk concentration of species A, mol/m^3
C_A^* = dimensionless concentration of species A ($= C_A/C_{A,s}$)
C_c = carbon concentration, mol/m^3
C_c^0 = initial carbon concentration, mol/m^3
C_c^* = dimensionless carbon concentration ($= C_c/C_c^0$)
D = overall diffusion constant, m^2/s
D_e = effective diffusivity, m^2/s
D_f = bulk diffusivity, m^2/s
D_K = Knudsen diffusivity, m^2/s
d = pore diameter, m
d_0 = initial char particle diameter, m
E = activation energy, kJ/mol
E_0 = activation energy at $\epsilon = 0$, kJ/mol
h = classic Thiele modulus
k = intrinsic reaction rate constant based on surface area, m/s

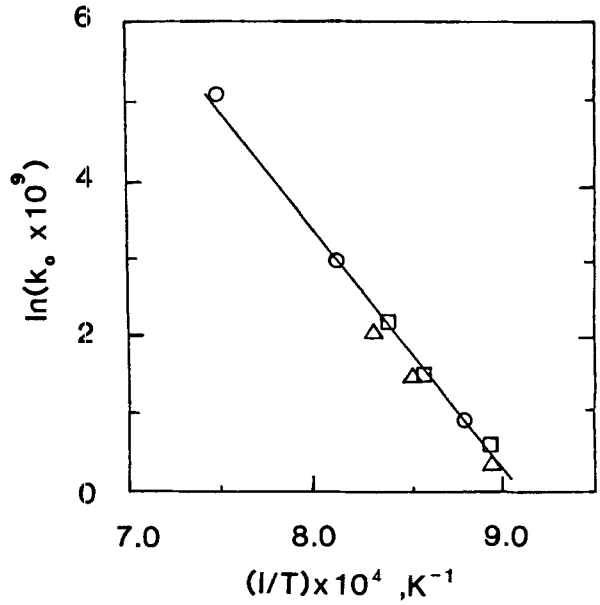

Figure 12. Arrhenius plot for CO_2 gasification of the three different chars: □, Montana Rosebud; △, Illinois No. 6; O, Hydrane No. 49 char.

k_c = thermal conductivity of continuous medium, J/m·s·K
k_0 = intrinsic reaction rate constant at $\epsilon = 0$, m/s
M_a = mass of ash in char sample, kg
M_s = mass of char sample, kg
M_v = mass of volatile matter in char sample, kg
n = apparent reaction order
P = pressure, Pa
q = ratio of gaseous concentration to solid concentration ($= C_{A,s}/C_c^0$)
R = particle radius, m
R = universal gas constant, 0.0083164 kJ/mol·K
r = radial distance from the center of particle, m
r^* = dimensionless radius ($= r/R$)
S = a constant defined in Eq. 5
S_g = specific surface area, m^2/kg or m^2/g
T = temperature, K
T_r = reference temperature, K
T_b = bulk temperature, K
T^* = dimensionless temperature ($= T/T_b$)
t = real time, s
$t_{0.5}$ = time when $X = 0.5$, s
t^* = dimensionless time
v = pore volume of particle, m^3/kg
X = overall conversion
$\hat{X}$ = fractional conversion defined by Eq. 43
X = fractional conversion defined by Eq. 44
X_{MN} = overall conversion where the minimum in the rate occurs
X_{MX} = overall conversion where the maximum in the rate occurs
x = local carbon conversion

Greek Letters

α_T = dimensionless number defined in Eq. 39
γ = a constant
δ = dimensionless number ($= E_0/RT_b$)
ϵ = porosity
ρ_p = particle apparent density, kg/m^3
ρ_t = particle true density, kg/m^3
τ^* = dimensionless time
τ_m = tortuosity
ϕ = a modified Thiele modulus
ψ = a function introduced in Eq. 22

LITERATURE CITED

Angus, J. C., et al., "Thermogravimetric Measurements At High Pressures Using a Hanging Reactor Thermobalance," Annual Meeting of AIChE, Paper No. 12b, Chicago (Nov. 16–20, 1980).

Aris, R., *Elementary Chemical Reactor Analysis*, Prentice-Hall, Englewood Cliffs, NJ (1969).

Badzioch, S., D. R. Gregory, and M. A. Field, "Investigation of the Temperature Variation of the Thermal Conductivity and Thermal Diffusivity of Coal," *Fuel*, **43**, 267 (1964).

Bischoff, K. B., "Accuracy of the Pseudo Steady State Approximation for Moving Boundary Diffusion Problems," *Chem. Eng. Sci.*, **18**, 711 (1963).

Blackwood, J. D., and A. J. Ingeme, "The Reaction of Carbon with Carbon Dioxide at High Pressure," *Aust. J. Chem.*, **13**, 194 (1960).

Dutta, S., C. Y. Wen, and R. J. Belt, "Reactivity of Coal and Char. 1. In Carbon Dioxide Atmosphere," *Ind. Eng. Chem. Process Des. Dev.*, **16**, No. 1, 20 (1977).

Feldkirchner, H. L., and J. Huebler, "Reaction of Coal with Steam-Hydrogen Mixtures at High Temperatures and Pressures," *Ind. Eng. Chem. Process Des. Dev.*, **4**, 134 (1965).

Gan, H., S. P. Nandi, and P. L. Walker, Jr., "Nature of the Porosity in American Coals," *Fuel*, **51**, 272 (1972).

Gardner, N. C., J. J. Leto, S. Lee, and J. C. Angus, "Thermogravimetric Measurements at High Pressures," *NBS Special Publication*, **580**, 235 (1980).

Ishida, M., and C. Y. Wen, "Comparison of Kinetic and Diffusional Models for Solid-Gas Reactions," *AIChE J.*, **14**, No. 2, 311 (1968).

Laurendeau, N. M., "Heterogeneous Kinetics of Coal Char Gasification and Combustion," *Prog. Energy Combust. Sci.*, **4**, 221 (1978).

Lee, S., "Coal Char Gasification Studies," Ph.D. Dissertation, Case Western Reserve University (1980).

Mahajan, O. P., R. Yarzab, and P. L. Walker, Jr., "Unification of Coal-Char Gasification Reaction Mechanisms," *Fuel*, **57**, 643 (1978).

Marsh, H., "The Determination of Surface Areas of Coals—Some Physicochemical Considerations," *Fuel*, **44**, 253 (1965).

Petersen, E. E., "Chemical Reaction Analysis," Prentice-Hall, Englewood Cliffs, NJ (1965).

Walker, Jr., P. L., F. Rusinko, Jr., and L. G. Austin, *Advances in Catalysis*, **XI**, 133, Academic Press, New York (1959).

Wicke, E., "Contributions to the Combustion Mechanism of Carbon," Fifth Symp. on Combustion, 245, Reinhold, New York (1955).

Manuscript received January 20, 1983; revision received May 26, and accepted July 1, 1983.

Liquid-Phase Diffusion and Adsorption of Pyridine in Porous Silica-Alumina Pellets

The adsorption and effective diffusivity of pyridine dissolved in heptane were measured in silica-alumina pellets using a specially developed single-pellet continuous-flow diffusion cell. The measured diffusivities varied between 0.43×10^{-9} and 3.25×10^{-9} $m^2 \cdot s^{-1}$; the temperature dependence of the diffusivities indicated that both pore volume diffusion and surface diffusion play a role in the mass transfer.

D. S. van VUUREN

Chemical Engineering Research Group—CSIR
Pretoria, Republic of South Africa

C. M. STANDER

National Physical Research Laboratory—CSIR
Pretoria, Republic of South Africa

DAVID GLASSER

Dept. of Chemical Engineering
University of the Witwatersrand
Johannesburg, Republic of South Africa

SCOPE

The heterocyclic nitrogen compounds present in fossil-fuel liquids like shale oils, petroleum and coal liquids cause problems such as catalyst poisoning during processing and formation of excessive nitrogen compounds during the combustion of the final products. Their removal by hydrodenitrogenation in multiphase reactors or possibly by liquid-phase adsorption in a packed column is, therefore, essential.

Mass transfer effects such as bulk diffusion in the pores and adsorption accompanied by surface diffusion on the pore walls of catalysts have a major influence on the efficiency of these removal processes. It is, therefore, important to establish the magnitude of the effective diffusivities and adsorption coefficients in these systems by either predictive or experimental methods. The available predictive methods for determining effective diffusivities are not adequate in systems where adsorption and surface diffusion are important and experimental methods must therefore be used. This paper describes a novel way to determine effective liquid-phase diffusivities in porous solids by measuring the transient response in a single-pellet continuous-flow system.

CONCLUSIONS AND SIGNIFICANCE

Using the developed method, the effective diffusivities of pyridine in the porous silica-alumina materials were measured to an estimated accuracy of about 20%. Advantages of the technique are: sampling is easy (even at elevated temperatures where evaporation of the liquids can cause experimental difficulties); only small amounts of fluid are required; there is no

Correspondence concerning this paper should be addressed to D. S. van Vuuren.